Appl Biochem Biotechnol (2011) 165:1507–1518
DOI 10.1007/s12010-011-9371-3

The Binding Sites of Class I Release Factor (eRF1) Toward Class II Release Factor (eRF3) in *Euplotes octocarinatus*

Jie Chen · Yue-jun Fu · Bing-sheng Yang · Yan-bo Wu · Ai-hua Liang

Received: 30 October 2010 / Accepted: 5 September 2011 /
Published online: 22 September 2011

Abstract The C domain of eRF1 interacts with the C domain of eRF3, and the binding of both factors is essential for fast kinetics of the termination of protein translation. Analysis by computational simulation demonstrated that several peptides involved in Eo-eRF1/Eo-eRF3 interaction directly. Among these peptides, the two motifs GVEDT and GFGG were highly conserved, while the fragment aa338-346 of Eo-eRF1a/b was variable. In additional, I290 and D293 of Eo-eRF1 were also highly conserved. By the site-directed mutagenesis and pull-down analysis, the amino acid D293 in Eo-eRF1bC domain was conformed playing an important role in eRF1–eRF3 interaction. Eo-eRF1a and Eo-eRF1b may select different manners to interact with Eo-eRF3. These studies contribute to the better understanding the mode of eRF1–eRF3 interaction.

Keywords eRF1–eRF3 interaction · Binding sites · Computational simulation

Abbreviations

eRF1	Class I polypeptide release factor in eukaryotes
eRF3	Class II polypeptide release factor in eukaryotes
Bj-eRF1	Class I polypeptide release factor in *Blepharisma japonicum*
Eo-eRF1a	Class I polypeptide release factor a in *Euplotes octocarinatus*
Eo-eRF1b	Class I polypeptide release factor b in *E. octocarinatus*
Hs-eRF1	Class I polypeptide release factor in *Homo sapiens*
Bj-eRF1C	C domain of Bj-eRF1 (274–436)

Electronic supplementary material The online version of this article (doi:10.1007/s12010-011-9371-3) contains supplementary material, which is available to authorized users.

J. Chen · Y.-j. Fu · A.-h. Liang (✉)
Key Laboratory of Chemical Biology and Molecular Engineering of Ministry of Education,
Institute of Biotechnology, Shanxi University, Taiyuan 030006, China
e-mail: aihualiang@yahoo.com

B.-s. Yang · Y.-b. Wu
Key Laboratory of Chemical Biology and Molecular Engineering of Ministry of Education,
Institute of Molecular Science, Shanxi University, Taiyuan 030006, China

Eo-eRF1aC	C domain of Eo-eRF1a (270–446)
Eo-eRF1bC	C domain of Eo-eRF1b (270–437)
Eo-eRF3	Class II polypeptide release factor in *E. octocarinatus*
Eo-eRF3Cm6	Truncated peptide of Eo-eRF3 (640–723)
Bj-eRF1C/Eo-eRF3Cm6	Heterodimeric complex of Bj-eRF1C and Eo-eRF3Cm6
Eo-eRF1aC/Eo-eRF3Cm6	Heterodimeric complex of Eo-eRF1aC and Eo-eRF3Cm6
Eo-eRF1bC/Eo-eRF3Cm6	Heterodimeric complex of Eo-eRF1bC and Eo-eRF3Cm6
MD	Molecular dynamics
RLS	Resonance light scattering

Introduction

Protein translation termination occurs when one of three stop codons, UAA, UAG, or UGA, enters the ribosomal A site. Two classes of release factors mediate this process in both prokaryotes and eukaryotes, although the mechanisms are quite distinct. In eukaryotes, translation is terminated by a heterodimer consisting of two proteins, release factors eRF1 and eRF3, which interact in vivo [1]. The eukaryotic class I release factor eRF1 recognizes all stop codons and triggers peptidyl-tRNA hydrolysis to release the nascent peptide from the ribosome [1]. eRF1 proteins from eukaryotic species share significant homology at the primary amino acid sequence level. The human eRF1 structure, in a crystal structure [2] and in solution [3], consists of three domains (N, M, and C domains). The C-terminal domain of eRF1 is known to interact with the C domain of eRF3 [4]. The binding complex of both factors, which appears to cause conformational changes in one or both factors, is essential for fast kinetics of the termination of translation [5, 6]. In vitro reconstitution of eukaryotic translation reveals that the pretermination complexes binding of eRF1, eRF3, and GTP induces a structural rearrangement revealed as a two-nucleotide forward shift of the toeprint; and these interactions lead to GTP hydrolysis followed by rapid hydrolysis of peptidyl-tRNA [6, 7].

Some organisms which deviate from the standard genetic code are called variant code organisms. For example, the ciliate *Blepharisma* and *Euplotes* species retain UAA and UAG as stop codons, but reassign UGA to tryptophan and cysteine, respectively [8, 9]. While, ciliate eRF1 proteins retain substantial overall amino acid sequence homology with eRF1s from standard code organisms, particular variations may account for the functional differences in these proteins. The highly conserved amino acid motifs in standard code organisms, which are more degenerate in variant code organisms, may represent key residues that mediate recognition to stop codons [2, 8, 10]. In recent studies, a hybrid eRF1 carrying the *Euplotes octocarinatus* domain N fused to *Saccharomyces cerevisiae* domains M and C (Eo/Sc eRF1) was constructed. The mutations in the TASNIKS motif (the highly conserved motif in N domain) of the hybrid (Eo/Sc eRF1) eliminated the eRF3 requirement for peptide release at terminal codons [5]. It was proposed that the highly conserved TASNIKS motif and eRF3 function together to trigger eRF1 conformational changes which couples stop codon recognition and polypeptide release during eukaryotic translation termination [5]. The helix $\alpha 1$ located in the N domain was presumed to be involved in the interaction between eRF1 and eRF3 [2]. Furthermore, the structure of triple complex eRF1–mRNA–tRNA was characterized by spatial proximity of stop codon nucleotides to the C domain of the eRF1 [11]. Taken together, eRF1–eRF3 interaction may play an important role in stop codon recognition.

E. octocarinatus has two genes encoding Eo-eRF1s: eRF1a and eRF1b [9]. Both Eo-eRF1s had a similar function in *E. octocarinatus* [12]. It was previously shown that a short portion of the C-terminal domain of eRF3 (Eo-eRF3Cm6) was sufficient for Eo-eRF1a binding in *E. octocarinatus* [13]. In this study, the interaction between Eo-eRF1bC and Eo-eRF3Cm6 was confirmed by pull-down, Western blot assays, and resonance light scattering (RLS). Then, the binding regions on Eo-eRF1aC, Eo-eRF1bC, and Bj-eRF1C toward Eo-eRF3Cm6 were inferred by computational docking simulation. Finally, a key amino acid in eRF1–eRF3 interaction was tested by site-directed mutagenesis and pull-down analysis.

Materials and Methods

Computational Simulation of the Interaction Between Eo-eRF1a/b C and Eo-eRF3Cm6

The atomic coordinates of HeRF1 C domain [Protein Data Bank (PDB) code, 2KTV] [14] and HeRF1/eRF3-23 complex (PDB code, 3E1Y) [15] were downloaded from the PDB www.rcsb.org/pdb). The homologous spatial structure of Eo-eRF1b C/eRF3Cm6 complex was modeled by using the crystal structures of HeRF1/eRF3-23 complex as templates through the SWISS-MODEL server [16–18]. The 3D HeRF1/eRF3-23 complex (PDB code, 3E1Y) structure does not contain information about the unresolved region (aa351-370) of the HeRF1 C domain, so the atomic coordinates of this region were replaced by that of the same region in the NMR structure of Hs-eRF1 C domain (PDB code, 2KTV). The modeled Eo-eRF1bC/eRF3Cm6 complex structure was used for molecular dynamics simulation. The modeled 3D structure was refined by optimization (steepest descent, conjugate gradient, and VA09A minimization) and 500 steps of conjugate gradient minimization within a 10 Å water box model. Molecular dynamics (MD) simulation was performed to examine the quality of the model structure via 5 ps with the step size of 1 fs at a constant temperature of 298 K. The simulation mentioned above was accomplished without constraints under the consistent valence force field by Discover-3 software package in the InsightII program (Accelrys; www.accelrys.com/products/insight). The total energy is obtained from the results of the optimization by InsightII program. The DeepView, the Swiss-Pdb Viewer V.3.7 software, was used to view and analyze the molecular graphics of modeled proteins or protein complex structures. Hydrogen bond computation, electrostatics, and non-bound energy computations were done with the GROMOS96 implementation of Swiss-PdbViewer. The same protocols were used for computational simulation of the complexes Bj-eRF1C/Eo-eRF3Cm6 and Eo-eRF1aC/Eo-eRF3Cm6.

Strains and Media

Bacteria were grown in LB broth (1% bactotryptone, 0.5% yeast extract, and 0.5% NaCl) [19] supplemented with relevant antibiotics (50 μg/ml ampicillin or 50 μg/ml kanamycin) for selection.

Plasmid Constructs

Plasmid pRSETC-Eo-eRF1aC (aa270-446), pRSETC-Eo-eRF1bC (aa274-437), and pRSETC-Bj-eRF1C (aa274-436) were constructed by insertion of a *Nhe* I/*Xho* I digested PCR product into the same sites of pRSETC (Invitrogen). The PCR products were amplified by the proper primers (see Table 1) and plasmid Te-Eo-eRF1a [9]. Te-Eo-eRF1b

Table 1 The nonbonded and electrostatic energy of the predicted binding sites in Eo-eRF1b/Eo-eRF3Cm6 complex

Residue		Nonbonded energy (kJ/mol)			Electrostatic energy (kJ/mol)		
		Eo-eRF1b	Complex	ΔE	Eo-eRF1b	Complex	ΔE
ILE	290	−34.45	−40.82	−6.37	7.06	8.16	1.1
ASP	293	−29.96	−31.68	−1.72	7.55	5.11	−2.44
PHE	299	−45.46	−63.73	−18.27	32.96	30.55	−2.41
GLY	300	−44.09	−47.87	−3.78	31.09	32.58	1.49
VAL	301	−51.12	−62.86	−11.74	2.43	3.99	1.56
GLU	302	−50.83	−47.74	3.09	5.15	−8.28	−13.43
ASP	303	−41.82	−52.80	−10.98	5.47	10.74	5.27
ILE	324	−41.57	−57.34	−15.77	0.69	−5.15	−5.84
ASP	331	−25.78	−36.69	−10.91	21.23	18.79	−2.44
PRO	332	−21.44	−37.27	−15.83	−19.67	−17.63	2.04
LYS	338	−33.05	−35.58	−2.53	−11.5	−9.5	2
ILE	339	−50.21	−52.88	−2.67	−0.56	−3.37	−2.81
TYR	340	−28.49	−52.76	−24.27	−57.6	−41.43	16.17
ASN	341	−30.78	−48.25	−17.47	−166.28	−166.38	−0.1
LEU	342	−29.28	−50.91	−21.63	−1.02	−10.75	−9.73
ASN	343	−26.40	−43.99	−17.59	−161.36	−163.26	−1.9
LYS	344	−34.12	−49.45	−15.33	−11.59	0.69	12.28
GLU	345	−25.80	−24.00	1.8	4.54	−1.4	−5.94
GLN	346	−19.26	−33.47	−14.21	−179.68	−166.27	13.41
GLU	347	−35.83	−40.91	−5.08	6.37	4.32	−2.05
LYS	348	−31.04	−41.46	−10.42	9.4	17.2	7.8
ASP	349	−26.40	−40.32	−13.92	0.75	13.32	12.57
ASN	400	−42.79	−58.56	−15.77	−125.48	−134.18	−8.7
GLY	401	−39.60	−35.31	4.29	40.56	34.31	−6.25
PHE	402	−46.88	−49.19	−2.31	32.93	28.32	−4.61
GLY	404	−10.84	−18.83	−7.99	20	30.19	10.19
Total energy		−897.29	−1154.67	−257.38	−506.56	−489.33	17.23

[9] and pRSETC-Bj-eRF1 [20] were used as templates. The *E. octocarinatus eRF1b* gene contains three UGA (297, 384, and 1125) stop codons that are reassigned for cysteine [9]. The last one (UGA 1125) is located in its C domain. In order to express the C domain of *Eo-eRF1b* gene in *Escherichia coli*, the UGA 1125 was mutated to the standard cysteine code UGT. Site-directed mutagenesis was introduced by using the TaKaRa Mutant Best kit (TaKaRa Biotechnology Co., Ltd., Dalian, China). A highly conservative aspartic acid (293 in Eo-eRF1a/b and 297 in Bj-eRF1) was mutated to asparagines and valine. All mutants were verified by DNA sequencing analysis.

Protein Expression, Purification, and In Vitro Pull-down Analysis

The plasmid pRSETC-Eo-eRF1bC (aa274-436) was transformed into strain *E. coli* BL21 (DE3). Transformants were grown to an OD_{600} value of 0.4–0.6 at 37 °C and induced with

0.1 mM isopropyl-1-thio-β-D-galactoside for 15 h at 16 °C. Cells were harvested, lysed by sonication on ice, and centrifuged at 12,000×*g* for 15 min. The supernatant-containing soluble recombinant Eo-eRF1bC was saved for purification. Purification of recombinant Eo-eRF1bC and Western blot analysis were carried out as previously described [23???] with minor modifications. The same conditions and protocols were used for transformation, growth, and induction with the following plasmids: pRSETC-Eo-eRF1aC (aa274-436), pRSETC-Bj-eRF1C (aa274-436), and their mutants. Preparation of protein complexes of eRF1C and truncated Eo-eRF3Cm6 (640-723) and in vitro pull-down analysis were carried out as previously described [13] with minor modifications.

Resonance Light Scattering

The RLS spectrum was recorded with a F-2500 fluorescence spectrophotometer by scanning simultaneously the excitation and emission spectra from 250.0 to 600.0 nm with $\Delta\lambda$=0 nm and a slit width of 5.0 nm.

Results

Computational Simulation

The spatial structure of Eo-eRF1b/eRF3Cm6 complex was modeled by using the crystal structures of HeRF1/eRF3-23 complex as templates. Because both interactional proteins were treated as rigid bodies, the effect of residue flexibility was considered negligible. Energy minimization and 5-ps MD simulations of each mode were performed to improve the docking performance. Then, the total energy of the modeled structures was calculated. The same protocols were used for computational simulation of the complexes Bj-eRF1C/Eo-eRF3Cm6 and Eo-eRF1aC/Eo-eRF3Cm6. The total energy of the modeled structures Eo-eRF1bC/eRF3Cm6, Eo-eRF1aC/eRF3Cm6, and Bj-eRF1C/Eo-eRF3Cm6 were 8,503, 8,624, and 8,549 kJ/mol. The data of complexes Eo-eRF1bC/eRF3Cm6, Eo-eRF1aC/Eo-eRF3Cm6, and Bj-eRF1C/Eo-eRF3Cm6 are also shown in Tables 1, 2, and 3.

Table 1 shows that after binding with Eo-eRF3Cm6, the nonbonded energy of probable binding sites in Eo-eRF1bC complex decreases the total energy by 257.38 kJ/mol, while the electrostatic energy increases the total energy by 17.23 kJ/mol. We can conclude that the nonbonded interaction between Eo-eRF1bC and Eo-eRF3Cm6 is propitious to forming the complex for decreasing the total energy. Bj-eRF1C is the similar situation (Table 3). But in Eo-eRF1aC complex, it was showed that after binding with Eo-eRF3Cm6, the nonbonded energy of probable binding sites in Eo-eRF1aC complex decreases the total energy by 117.2 kJ/mol, while the electrostatic energy decreases the total energy by 164.48 kJ/mol (Table 2). We can conclude that both the nonbonded and electrostatic interaction between Eo-eRF1aC and Eo-eRF3Cm6 are propitious to form the Eo-eRF1aC complex for decreasing the total energy.

The amino acid residues, which probably involved in eRF1–eRF3 interaction directly (shown in Tables 1, 2, and 3), were analyzed by sequence alignment. The result shows that two motifs GVEDT and GFGG were highly conserved, while the fragment aa338-346 of Eo-eRF1a/b was variable (Fig. 1). In addition, I290 and D293 of Eo-eRF1 were also highly conserved. Merkulova's research showed that 281–305 and 411–415 were important residues of eRF1–eRF3 interaction in a highly homologous human system [4]. The conserved motif GVEDT, I290, and D293 are just located in this region. In addition, D293 is the only

Table 2 The nonbonded and electrostatic energy of the predicted binding sites in Eo-eRF1a/Eo-eRF3Cm6 complex

Residue		Nonbonded energy (kJ/mol)			Electrostatic energy (kJ/mol)		
		Eo-eRF1a	Complex	ΔE	Eo-eRF1a	Complex	ΔE
ILE	290	−24.36	−23.53	0.83	7.53	1.56	−5.97
ASP	293	−27.14	−30.06	−2.92	−3.98	0.7	4.68
PHE	299	−49.23	−48.44	0.79	33.36	37.08	3.72
ILE	301	−19.31	−21.76	−2.45	−1.98	−5.46	−3.48
GLU	302	−28.81	−36.01	−7.2	−10.46	26.39	36.85
ASP	303	−33.1	−45.54	−12.44	3.15	13.42	10.27
ASN	306	−40.81	−41.59	−0.78	−163.93	−161.88	2.05
GLU	309	−39.11	−34.72	4.39	2.6	0.89	−1.71
LEU	310	−45.16	−37.75	7.41	33.14	40.69	7.55
PRO	332	−30.32	−25.06	5.26	−18.51	−33.67	−15.16
SER	333	−49.11	−39.64	9.47	61.53	−23.22	−84.75
GLU	335	−33.83	−28.56	5.27	9.01	−1.49	−10.5
GLU	336	−68.3	−68.59	−0.29	−4.06	0	4.06
ILE	337	−37.36	−42.48	−5.12	−4.04	−3.33	0.71
LYS	338	−42.89	−42.61	0.28	−5.91	−5.09	0.82
ILE	340	−32.19	−30.16	2.03	−2.84	18.24	21.08
HIS	341	−34.27	−22.42	11.85	10.42	3.74	−6.68
CYS	343	−20.52	−40.19	−19.67	−2.14	−9.47	−7.33
ASP	349	−36.94	−27.62	9.32	−1.79	−3.58	−1.79
ARG	351	−16.85	−35.16	−18.31	−256.68	−255.97	0.71
ASP	356	−21.19	−39.6	−18.41	14.9	2.56	−12.34
ASN	357	−17.87	−36.17	−18.3	−165.71	−169.85	−4.14
TYR	359	−24.8	−29.5	−4.7	9.88	−46.12	−56
ILE	363	−13.94	−22.28	−8.34	10.64	10.54	−0.1
TYR	390	−51.17	−55.1	−3.93	−13.78	6.16	19.94
GLY	410	−24.36	−20.33	4.03	44.69	16	−28.69
PHE	411	−38.68	−53.87	−15.19	43.18	30.57	−12.61
GLY	412	−14	−23.39	−9.39	72.67	70.75	−1.92
GLU	425	−18.86	−22.61	−3.75	11.26	5.41	−5.85
ASN	426	−31.48	−47.99	−16.51	−148.12	−166.73	−18.61
ILE	427	−26.16	−36.59	−10.43	95.66	96.37	0.71
Total energy		−992.12	−1109.32	−117.2	−340.31	−504.79	−164.48

unanimous residue to form H-bond in Eo-eRF1a/b and Bj-eRF1 complex. To determine the effect of H-bond at D293 on eRF1–eRF3 interaction, we carry out point mutation analysis.

Protein Expression, Purification, and In Vitro Interaction

The fusion protein Eo-eRF1bC-His_6 was expressed and purified. The estimated molecular mass of the fusion protein product Eo-eRF1bC-His_6 was nearly 19 kDa (Fig. 2a, *lane 3*), which was identical to the calculated molecular mass.

Table 3 The nonbonded and electrostatic energy of the predicted binding sites in Bj-eRF1/Eo-eRF3Cm6 complex

Residue		Nonbonded energy (kJ/mol)			Electrostatic energy (kJ/mol)		
		Bj-eRF1	Complex	ΔE	Bj-eRF1	Complex	ΔE
VAL	294	−31.5	−37.61	−6.11	5.43	3.77	−1.66
ASP	297	−27.33	−35.86	−8.53	−4.85	3.92	8.77
TYR	303	−59.38	−68.26	−8.88	−34.56	−18.14	16.42
GLY	304	−24.96	−26.08	−1.12	25.77	36.95	11.18
VAL	305	−31.4	−44.83	−13.43	0.31	2.11	1.8
GLU	306	−34.89	−53.76	−18.87	4.95	2.83	−2.12
ASP	307	−43.5	−45.76	−2.26	6.05	2.88	−3.17
PHE	323	−58.38	−62.55	−4.17	−2.45	6.92	9.37
ASN	325	−23.97	−27.6	−3.63	−166.17	−166.78	−0.61
VAL	340	−20.91	−37.89	−16.98	−4.49	−1.55	2.94
GLU	341	−32.25	−40.26	−8.01	−5.82	1.69	7.51
LYS	342	−49.04	−57.57	−8.53	−5.32	−9.12	−3.8
THR	343	−30.13	−42.05	−11.92	−11.41	−14.55	−3.14
LEU	344	−45.1	−53.14	−8.04	−14.32	−14.22	0.1
TYR	345	−59.7	−71.26	−11.56	−48.02	−43.59	4.43
LEU	346	−51.6	−51.45	0.15	−8.24	−10.28	−2.04
THR	347	−30.7	−29.32	1.38	21.93	5.74	−16.19
GLU	349	−28.56	−37.13	−8.57	5.73	−17.53	−23.26
ASP	355	−29.21	−32.9	−3.69	7.68	8.74	1.06
MET	358	−22.3	−32.29	−9.99	2.1	7.67	5.57
GLU	359	−35.05	−57.04	−21.99	2.26	−5.13	−7.39
GLY	403	−11.26	−22.41	−11.15	44.01	43.06	−0.95
PHE	404	−50.93	−57.07	−6.14	37.05	41.18	4.13
GLY	405	−13.37	−20.18	−6.81	71.09	69.35	−1.74
GLY	406	−16.52	−23.45	−6.93	32.61	47.42	14.81
Total energy		−861.94	−1067.72	−205.78	−38.68	−16.66	22.02

To test whether Eo-eRF1bC could bind to the eRF3Cm6 protein of *E. octocarinatus*, pull-down analysis was carried out. The glutathione *S*-transferase (GST)-Eo-eRF3Cm6 fusion protein was first immobilized onto glutathione Sepharose 4B beads, followed by incubation with the Eo-eRF1bC-His_6 sample. After washing the beads with binding buffer to remove the non-specific binding proteins, the complex Eo-eRF1bC-His_6/GST-Eo-eRF3Cm6 was eluted by glutathione and analyzed by Western blot with an 6×His tag antibody (Fig. 2b). The result indicated that immobilized GST-Eo-eRF3Cm6 could form a specific complex with Eo-eRF1bC-His_6 from the supernatant containing recombinant Eo-eRF1bC-His_6. The purified Eo-eRF1bC/Eo-eRF3Cm6 complex was used in following analysis.

D293, a highly conserved in Eo-eRF1, is the only unanimous residue to form H-bond in Eo-eRF1a/b and Bj-eRF1 complex. To determine the effect of H-bond at D293 on eRF1–eRF3 interaction, we carry out point mutation analysis. Each mutation was expressed, and then pull-down analysis was carried out. Unless binding with Eo-eRF3Cm6, eRF1C and

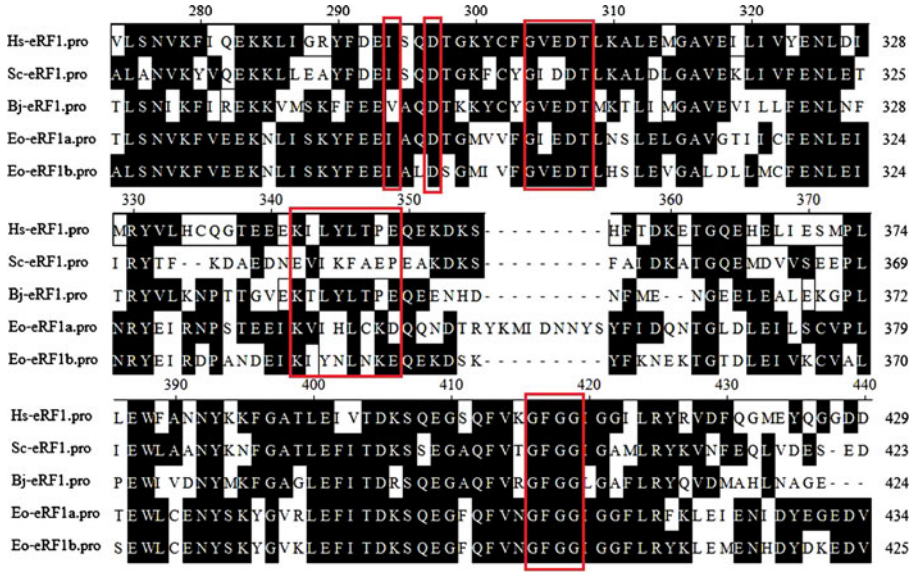

Fig. 1 The sequence alignment of eRF1C from different species. Identical amino acid residues are highlighted as *black bold face*. *Panes* indicate highly conservative binding region

their mutations could not present in pull-down analysis. Western blot was carried out to analyze the relevant quantity of eRF1C and their mutations. For the difficult to keep consistency of the amount of GST-Eo-eRF3Cm6, it was not accurate to determine the amount eRF1C directly. In order to erase the experiment error, the mutation complexes were analyzed by 6× His tag antibody and GST antibody in Western blotting analysis, respectively. The anti-GST antibody was used to detect the total amount of GST-Eo-eRF3Cm6, while the anti-His_6 antibody was used to detect the amount of eRF1C in purified

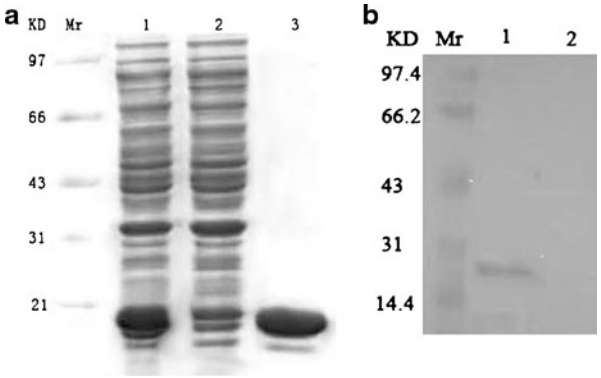

Fig. 2 Expression, purification, and Western blot analysis of Bj-eRF1C. **a** *Lane 1*, *E. coli* BL21 (DE3)/pRSETc-Eo-eRF1bC whole cell proteins after induction; *lane 2*, *E. coli* BL21 (DE3)/pRSETC-Eo-eRF1bC whole cell proteins supernatant suspension after induction; *lane 3*, Eo-eRF1bC eluted from Ni-NTA-agarose. **b** Western blot of Eo-eRF1bC using anti-His antibody and peroxidase-conjugated goat anti-mouse IgG. *Mr* prestained protein ladder; *lane 1* Eo-eRF1bC binding to Eo-eRF3Cm6; *lane 2* GST (negative control)

complexes. The wild-type Eo-eRF1Bc/Eo-eRF3Cm6 complex was selected as control. According to the gray quantity of each blot, compared to wild-type Eo-eRF1bC/Eo-eRF3Cm6 complex, the relevant level of GST tag and His6 tag was obtained. The ratio of relevant level of His6 tag to that of GST tag indicated the capability of Eo-eRF1C and their mutation binding with Eo-eRF3Cm6. As shown in Fig. 3, each of the mutant eRF1 could bind with Eo-eRF3Cm6. According to the gray quantity of each blot, compared to wild-type Eo-eRF1bC, the homologous mutations D293N and D293V exhibit the decreased level in binding with Eo-eRF3Cm6. The binding rates in the complexes were about 57% (0.8/1.4= 0.57) and 40% (0.4/1=0.4), respectively. The binding capacity of Eo-eRF1aC-His_6 and Bj-eRF1C-His_6 and their homologous mutations (D293N and D293V in Eo-eRF1aC-His_6; D297N and D297V in Bj-eRF1bC-His_6) with Eo-eRF3Cm6 were also analyzed. The wild Eo-eRF1aC, Eo-eRF1bC, and Bj-eRF1C exhibit same binding capacity. Compared to the wild Eo-eRF1aC-His_6, the two mutations D293N and D293V of Eo-eRF1aC-His_6 exhibit a similar binding capacity (86% and 83%, respectively) with Eo-eRF3Cm6. The two mutations D293N and D293V of Bj-eRF1C-His_6 exhibit lower binding capacity (29% and 14%, respectively) with Eo-eRF3Cm6 than that of Eo-eRF1bC-His_6. The results suggested that the highly conservative aspine (D293 in Eo-eRF1C and D297 in Bj-eRF1C) played an important role in eRF1–eRF3 interaction.

Resonance Light Scattering

To determine the effect of the electrostatic interaction on complexes, we carried out RLS measurement under different salt concentration. Figure 4a shows the RLS spectra of complexes Bj-eRF1C/Eo-eRF3Cm6, Eo-eRF1aC/Eo-eRF3Cm6, and Eo-eRF1bC/Eo-eRF3Cm6. As presented from curves 1–3, all complexes have stronger RLS signals over the whole wavelength range of 250–450 nm. The RLS signal was observed a maximum at 368.0 nm (Fig. 4a). The RLS intensity was measured under different NaCl concentration from 0.05 to 0.9 M, and the results show that the RLS intensity decreased with increasing NaCl concentration. For the complexes Bj-eRF1C/Eo-eRF3Cm6 and Eo-eRF1bC/Eo-eRF3Cm6, the RLS intensity decreased when NaCl concentration was beyond 0.4 M, while the RLS intensity of Eo-eRF1aC/Eo-eRF3Cm6 decreased when NaCl concentration was beyond 0.25 M (Fig. 4b). These results indicated that Eo-eRF1aC/Eo-eRF3Cm6 is more

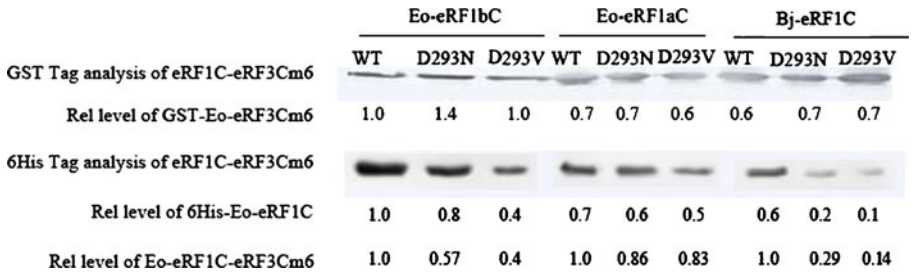

Fig. 3 Western blot quantitation of eRF1s and mutation binding with Eo-eRF3Cm6. The anti-GST antibody was used to detect the total amount of GST-Eo-eRF3Cm6, while the anti-His6 antibody was used to detect the amount of eRF1C in purified complexes. The wild-type Eo-eRF1bC/Eo-eRF3Cm6 complex was selected as control. According to the gray quantity of each blot, compared to wild-type Eo-eRF1bC/Eo-eRF3Cm6 complex, the relevant level of GST tag and His_6 tag were obtained, and the values were listed below the figures. The ratio of relevant level of His6 tag to that of GST tag indicated the capability of Eo-eRF1C and their mutation binding with Eo-eRF3Cm6

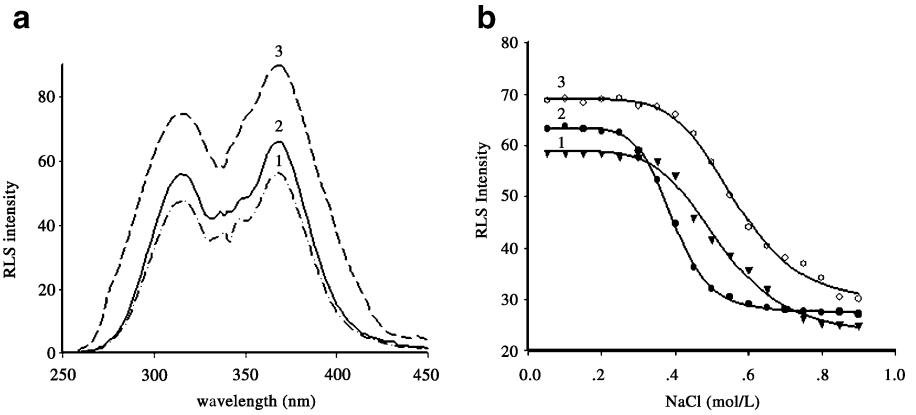

Fig. 4 Resonance light scattering spectrum of Bj-eRF1C/Eo-eRF3Cm6, Eo-eRF1aC/Eo-eRF3Cm6, and Eo-eRF1b C/Eo-eRF3Cm6 complex. **a** RLS spectra of Bj-eRF1C/Eo-eRF3Cm6 complex (*curve 1*), Eo-eRF1aC/Eo-eRF3Cm6 complex (*curve 2*), and Eo-eRF1b C/Eo-eRF3Cm6 complex (*curve 3*). Concentration: Bj-eRF1C/Eo-eRF3Cm6 0.06 mM, Eo-eRF1aC/Eo-eRF3Cm6 0.07 mM, and Eo-eRF1bC/Eo-eRF3Cm6 0.1 mM. **b** Effect of NaCl on the RLS intensity of Bj-eRF1C/Eo-eRF3Cm6 complex (*curve 1*), Eo-eRF1aC/Eo-eRF3Cm6 complex (*curve 2*), and Eo-eRF1b C/Eo-eRF3Cm6 complex (*curve 3*). Concentration: Bj-eRF1C/Eo-eRF3Cm6 0.06 mM, Eo-eRF1aC/Eo-eRF3Cm6 0.07 mM, and Eo-eRF1bC/Eo-eRF3Cm6 0.1 mM

sensitive to NaCl concentration than Bj-eRF1C/Eo-eRF3Cm6 and Eo-eRF1bC/Eo-eRF3Cm6. A probable reason is that electrostatic interaction contributes more in complex Eo-eRF1aC/Eo-eRF3Cm6 than in complexes Bj-eRF1C/Eo-eRF3Cm6 and Eo-eRF1bC/Eo-eRF3Cm6. These results were corresponded with the conclusion from computational simulation.

Discussion

Bj-eRF1 and Eo-eRF1a/b retain UAA and UAG as stop codons, but reassign UGA to tryptophan and cysteine, respectively [8, 9]. Bj-eRF1C is ~66.7% and 68.3%, homologous to Eo-eRF1aC and Eo-eRF1bC, respectively. Eo-eRF3Cm6 was tested to be the smallest polypeptide to bind with Eo-eRF1a [13]. Our result shows that Eo-eRF1b can also bind with Eo-eRF3Cm6. In addition, Eo-eRF1a/b and Bj-eRF1 have the similar capacity binding with Eo-eRF3Cm6.

The binding sites of Eo-eRF1 to Eo-eRF3Cm6 were analyzed by computational simulation. The result shows that the binding sites on Eo-eRF1 with eRF3 is consistent with previous reports in human and *Schizosaccharomyces pombe* [15], in which the Sp-eRF1 mutations F288A, I291A, Q400A, and F405A were shown reducing their binding to eRF3 by at least sixfold. Cheng's results showed that the surface groove on the domain C of eRF1 that interacts with domain 3 of eRF3 is composed mainly of hydrophobic amino acids. In addition to these predominant hydrophobic interactions, several residues of domain C in eRF1 contact residues of domain 3 in eRF3 through van der Waals interactions. In our research, the results from computational simulation suggested that the nonbonded interaction is predominant interaction. But, in Eo-eRF1aC complex, the electrostatic interaction is greater than that of Eo-eRF1bC and Bj-eRF1C complex. The RLS measurement was carried out under different salt concentration. The result shows that Eo-eRF1aC complex depolymerizes at lower NaCl concentration (0.25 M), while Eo-eRF1bC

and Bj-eRF1C complex depolymerize at higher NaCl concentrate (0.4 M). It implied that Eo-eRF1aC complex was sensitive to ionic strength. Ionic strength may affect the protein interaction by changing the microenvironment of hydrophilic residues. The results from RLS support the results from computational simulation. A probable reason is that electrostatic interaction contributes more in complex Eo-eRF1aC/Eo-eRF3Cm6. The result is corresponding with the conclusion from computational simulation. In recent study, the resonance assignment of hs-eRF1C domain indicates that the presence of two conformational (a closed and an open) states of residues 329-372 (minidomain) of Hs-eRF1, which is highly enriched in polar and charged residues [14]. In the closed conformers, the side chain of His356 is on the top of the α-helix and in closer contact with the negatively charged side chains of Glu365 and Glu367, whereas in the open conformer, His356 is closer to another charged side chain, that of Asp353, and the aromatic rings of Phe357 and Tyr331[14]. The main structural difference among the three complexes Eo-eRF1aC/eRF3Cm6, Bj-eRF1C/Eo-eRF3Cm6, and Eo-eRF1aC domain was showed in Fig S1. The Tyr331, Asp353, His356, Phe357, Asp365, and Glu367 in Hs-eRF1 were corresponding to the Tyr327, Asp349, His361, Phe362, Glu370, and Glu372 in Eo-eRF1aC, respectively. The results showed that Eo-eRF1aC is more similar to the open conformer, while Bj-eRF1C and Eo-eRF1bC are similar to the closed conformer. It was found that Eo-eRF1aC contains an extra peptide segment (aa352-360), which never experiences in other eRF1s (see Fig. 1). The extra peptide segment in Eo-eRF1aC was located in this minidomain mentioned above. The extra peptide segment is also highly enriched in polar and charged residues and just adjacent to the His361. Due to the insert of extra peptide segment, the conformer of minidomain in Eo-eRF1aC domain was changed. This change made Asp349 and His361 in Eo-eRF1aC domain far away from each other. So, the minidomain in Eo-eRF1aC domain is more similar to the open conformer. In additional, the polar and charged residues in the extra peptide segment of Eo-eRF1aC domain interacted with Eo-eRF3Cm6 decreased the total energy by 113.9 kJ/mol (Table 2). So, Eo-eRF1aC/eRF3Cm6 is more sensitive to NaCl concentration than Bj-eRF1C/Eo-eRF3Cm6 and Eo-eRF1bC/eRF3Cm6.

In protein interactions, the H-bond should not be neglected. In Tables S1S1, S2, and S3, the parameters of hydrogen bond in eRF1C/Eo-eRF3Cm6 complex were showed. We found that only one H-bond at Asp (D293 in Eo-eRF1a/b C and D297 in Bj-eRF1C) was conserved. In order to test the role of this Asp, amino acid replacement was employed. The side chain of valine has similar volume to that of aspartic acid without any electric charge and carbonyl group to form H-bond. The side chain of asparagine has no electric charge, but retains carbonyl group to form H-bond. When Asp replaced by Asn or Val, the binding capacity of eRF1C with Eo-eRF3Cm6 was decreased. So the conserved Asp is an important site for eRF1–eRF3 interactions. Our results show that the conserved Asp at Eo-eRF1bC and Bj-eRF1C was involved in eRF1–eRF3 interaction by both H-bond and electrostatic interaction. But in Eo-eRF1aC, amino acid replacement has little effect on eRF1–eRF3 interaction. From Tables S1, S2, and S3, we can find that D293 in Eo-eRF1bC and D297 in Bj-eRF1C forms H-bond with H473 in Eo-eRF3Cm6. The new H-bond shares similar bonding angle and bonding length. But D293 in Eo-eRF1aC forms H-bond with H713 in Eo-eRF3Cm6, in contradiction with that of Eo-eRF1bC and Bj-eRF1C.

From the above, we can draw a conclusion that Eo-eRF1aC, Eo-eRF1bC, and Bj-eRF1C can interact with Eo-eRF3Cm6. D293 in Eo-eRF1bC and D297 in Bj-eRF1C domain were conformed playing an important role in eRF1–eRF3 interaction. When binding with Eo-eRF3Cm6, Eo-eRF1bC shares similar characteristics with Bj-eRF1C. But the Eo-eRF1aC and Eo-eRF1bC interact with Eo-eRF3Cm6 with different manner.

Acknowledgments This work was supported by grants from the National Natural Scientific Foundation of China (Nos. 31071294, 30770294, and 30770295).

References

1. Frolova, L., Le Goff, X., Rasmussen, H. H., Cheperegin, S., Drugeon, G., Kress, M., et al. (1994). *Nature, 372*, 701–703.
2. Song, H., Mugnier, P., Das, A. K., Webb, H. M., Evans, D. R., Tuite, M. F., et al. (2000). *Cell, 100*, 311–321.
3. Kononenko, A. V., Dembo, K. A., Kiselev, L. L., & Volkov, V. V. (2004). *Molecular Biology (Mosk), 38*, 303–311.
4. Merkulova, T. I., Frolova, L. Y., Lazar, M., Camonis, J., & Kisselev, L. L. (1999). *FEBS Letters, 44*, 341–347.
5. Fan-Minogue, Hua, Du, Ming, Pisarev, A. V., Kallmeyer, A. K., Salas-Marco, J., Keeling, K. M., et al. (2008). *Molecular Cell, 30*, 599–609.
6. Salas-Marco, J., Bedwell, D. M. (2004). *Molecular Cellular Biology.* Sept. 7769–7778.
7. Alkalaeva, E. Z., Pisarev, A. V., Frolova, L. Y., Kisselev, L. L., & Pestova, T. V. (2006). *Cell, 125*, 1125–1136.
8. Lozupone, C. A., Knight, R. D., & Landweber, L. F. (2001). *Current Biology, 11*, 65–74.
9. Liang, A., Brünen-Nieweler, C., Muramatsu, T., Kuchino, Y., Beier, H., & Heckmann, K. (2001). *Gene, 262*, 161–168.
10. Kim, O., Yura, K., Go, N., & Harumoto, T. (2005). *Gene, 346*, 277–286.
11. Vorob'ev, I., Kiselev, L. L. (2008). *Molecular Biology (Mosk)*, 42341–351.
12. Wang, Y., Chai, B. F., Wang, W., & Liang, A. H. (2010). *Bioscience Reports, 30*, 425–431.
13. Song, L., Chai, B. F., Wang, W., & Liang, A. H. (2006). *Research in Microbiology, 157*, 842–850.
14. Mantsyzov, A. B., Ivanova, E. V., Birdsall, B., Alkalaeva, E. Z., Kryuchkova, P. N., Kelly, G., et al. (2010). *FEBS Journal, 277*, 2611–2627.
15. Cheng, Z. H., Saito, K., & Pisarev, A. V. (2009). *Genes & Development, 23*, 1106–1118.
16. Arnold, K., Bordol, L. (2006). The SWISS-MODEL Workspace: A web-based environment for protein structure homology modelling. *Bioinformatics*. 22195–201.
17. Schwede, T., & Kopp, J. (2003). *Nucleic Acids Research, 31*, 3381–3385.
18. Guex, N., & Peitsch, M. C. (1997). *Electrophoresis, 18*, 2714–2723.
19. Sambrook, J., Fritsch, E. F., & Maniatis, T. (2005). *Proteins, 60*, 207–221.
20. Wang, W., Chai, B. F., Heckmann, K., & Liang, A. H. (2004). *Biotechnology Letters, 26*, 959–963.